# PHASE RETRIEVAL FROM INCOMPLETE MAGNITUDE INFORMATION VIA TOTAL VARIATION REGULARIZATION

HUIBIN CHANG*, YIFEI LOU †, MICHAEL K. NG ‡, AND TIEYONG ZENG §

**Abstract.** The phase retrieval problem has drawn considerable attention, as many optical detection devices can only measure magnitudes of the Fourier transform of the underlying object (signal or image). This paper addresses the phase retrieval problem from incomplete data, where only partial magnitudes of Fourier transform are obtained. In particular, we consider structured illuminated patterns in holography, and find that non-integer values used in designing such patterns often yield better reconstruction than the conventional integer-valued ones. Furthermore, we demonstrate theoretically and numerically that three set of diffracted set of (complete) magnitude data are sufficient to recover the object. To compensate for incomplete information, we incorporate a total variation regularization to impose *a priori* to guarantee the reconstructed image satisfying some desirable properties. The proposed model can be solved efficiently by an alternative directional multiplier method with provable convergence. Numerical experiments validate the theoretical finding, and demonstrate the effectiveness of the proposed method in recovering objects from noisy and incomplete data.

**Key words.** Phase Retrieval; Partial Magnitudes; Total Variation; Alternative Directional Multiplier Method(ADMM)

**AMS subject classifications.** 46N10, 49N30, 49N45, 65F22, 65N21

## 1. Introduction.

When light waves pass by an object, far field measurements in terms of pointwise absolute value of the Fourier transform (FT) of the object can be obtained by Huygens' principle [25]. There are many applications involving such measurements, for instance, astronomical imaging [14], electron microscopy [36], and optics [43, 41], *etc.* As phase information is completely lost, the recovery of the underlying object $u$ from the magnitudes of its Fourier transform is referred to as *phase retrieval* (PR). In this work, we focus on reconstructing a 2D image $u$ defined on a discrete lattice $\Omega = \{0, 1, \cdots, n_1 \times n_2 - 1\} \to \mathbb{R}$ of size $n_1 \times n_2$ (note that we represent a 2D image in terms of a vector by the lexicographical order). The obtained data $b_0 : \Omega \to \mathbb{R}$ are magnitudes of the Fourier transform of $u$, *i.e.*, $b_0 = |\mathscr{F}u|$, where $\mathscr{F} : \mathbb{R}^{n_1 \times n_2} \to \mathbb{C}^{n_1 \times n_2}$ denotes the discrete Fourier transform (DFT)

$$(\mathscr{F}u)(\omega_1 + \omega_2 n_1) := \frac{1}{\sqrt{n_1 n_2}} \sum_{\substack{0 \le t_k \le n_k - 1, \\ k=1,2}} u(t_1 + t_2 n_1) \exp(-2\pi \mathbf{i}(\omega_1 t_1/n_1 + \omega_2 t_2/n_2)),$$

$\forall\ 0 \le \omega_k \le n_k - 1$, for $k = 1, 2$, where $\mathbf{i} = \sqrt{-1}$. As different images can have the same magnitudes, the PR problem does not have a unique solution, thus ill-posed.

One pioneer work of phase retrieve was proposed by Gerchberg and Saxton [22] using a projection-based error reduction method, which was later improved by a hybrid input-output algorithm proposed by Fienup [19]. Other projection-based variants include a hybrid projection-reflection method [2, 3], an iterated difference-map method

*School of Mathematical Sciences, Tianjin Normal University, Tianjin, 300387 China. E-mail: changhuibin@gmail.com

†Department of Mathematical Sciences, University of Texas at Dallas, Dallas, TX 75080, USA, E-mail: yifei.lou@utdallas.edu

‡Centre for Mathematical Imaging and Vision, and Department of Mathematics, Hong Kong Baptist University, Kowloon Tong, Hong Kong. Email: mng@hkbu.edu.hk

§Centre for Mathematical Imaging and Vision, and Department of Mathematics, Hong Kong Baptist University, Kowloon Tong, Hong Kong. Email: zeng@hkbu.edu.hk

[15], and relaxed averaged alternation reflections [30]. Alternatively, Machesini [34] adopted a saddle-point optimization to solve the PR problem, and a similar idea was presented in [44].

Major recent developments have been focused on semi-definite programming. For example, PhaseLift [9] reformulated the PR as a rank-one minimization problem, which was relaxed by a convex trace (nuclear) norm minimization. Waldspurger *et al.* [42] considered another convex relaxation technique, called PhaseCut, by splitting the phases and magnitudes via a complex semi-definite programming. Yin and Xin [47] proposed a nonconvex variant of PhaseLift by subtracting off Frobenius norm from the trace norm in PhaseLift, named as PhaseLiftOff, which successfully recovers signals with fewer measurements than PhaseLift numerically. A direct solver of the nonconvex PR problem was introduced in [8] and further developed in [12] where Wirtinger flow, a gradient scheme with novel update rules, was considered together with a careful initialization by means of a spectral method.

In this paper, we explicitly address the nonuniqueness issue of PR by acquiring two additional sets of data, thus yielding three sets in total:

$$M(u) := \{|\mathscr{F}u|, |\mathscr{F}(u + D^s u)|, |\mathscr{F}(u - \mathbf{i}D^s u)|\}, \tag{1.1}$$

where

$$(D^s u)(t_1 + t_2 n_1) = \exp\left(\frac{2\pi\mathbf{i}s_1 t_1}{n_1} + \frac{2\pi\mathbf{i}s_2 t_2}{n_2}\right) u(t_1 + t_2 n_1), \quad 0 \le t_k \le n_k - 1, k = 1, 2. \tag{1.2}$$

The data $M(u)$ can be obtained by illuminating the samples with three light fields: $\{1, 1 + \exp(2\pi\mathbf{i}s_1 t_1/n_1 + 2\pi\mathbf{i}s_2 t_2/n_2), 1 + \exp(2\pi\mathbf{i}s_1 t_1/n_1 + 2\pi\mathbf{i}s_2 t_2/n_2 - \mathbf{i}\pi/2\}$. It was proved in [7] that if both $s_1$ and $s_2$ in (1.2) are prime numbers (thus integers) with respect to $n_1$ and $n_2$ respectively, and each element of $|\mathscr{F}u|$ is non-zero, the signal $u$ can be exactly recovered from $3n_1n_2$ measurements. Unfortunately, $3n_1n_2$ measurements are often practically insufficient to recover the signal, and instead $7n_1n_2$ measurements are suggested by the authors. We find that if $s_1 = s_2 = 1/2$, then $3n_1n_2$ measurements yield an exact recovery of the PR problem, both theoretically and empirically. In particular, we assume the original image is non-negative, bounded, and real-valued; in other words, we assume that $u$ satisfies a $[0, 1]$ box constraint (up to scaling)[1]. We prove that $u$ can be uniquely determined from $3n_1n_2$ measurements for $s_1 = s_2 = 1/2$ in (1.2). We then demonstrate numerically that the unique solution can be obtained by solving a least-squares problem with a box constraint. Furthermore, we demonstrate that phase retrieval from incomplete information is possible. For this purpose, we formulate a variational model by introducing a total variation (TV) regularization, which is widely used in image processing since the seminal work of [39]. Recently, with the advance in compressive sensing (CS) [6], the TV regularization is provably efficient to recover signals or images from incomplete data or limited measurements [32, 33]. We employ an alternating direction of multipliers method (ADMM) [23, 45, 5, 10] or equivalently split Bregman method [24] to solve the TV-regularized minimization, followed by convergence analysis indicating that the algorithm converges to a stationary point. Numerical experiments show that the proposed method can recover the image from incomplete magnitude data and is stable to the presence of the noise.

[1] Such assumption was not needed in [7].

The rest of this paper is organized as follows. In Section 2, we present the uniqueness proof of the solution from $3n_1n_2$ measurements for $s_1 = s_2 = 1/2$ in (1.2). Both least-square and total variation models are examined in Section 3, while Section 4 discusses corresponding numerical algorithms with convergence analysis. Experiments are conducted in Section 5 to validate the theoretical aspects of the work, and demonstrate the robustness of the proposed method for image recovery from noisy and incomplete magnitude data. Finally, conclusions and future works are given in Section 6.

**2. Theoretical analysis.** It is straightforward that there exist three trivial ambiguities satisfying $b = |\mathscr{F}u|$ for different $u$: (1) multiplication by a complex constant with unit norm; (2) time-reversal(reflection); (3) shifted transformation (translation). Moreover, one can find infinitely many non-trivial solutions theoretically in [40]. To overcome the nonuniquesness issue, oversampling is often adopted [35, 37], *i.e.*, acquiring more samples in the frequency domain than that in the Nyquist frequency. Hayes [26] and Sanz [40] proved that if the underling signal is finitely supported and non-negative, then the solution of PR is uniquely determined from the number of measurements that is two times the dimension of the signal. The results are further extended under the setting of random oversampling [16, 17, 18], where random illumination was proposed to enforce absolute uniqueness and resolve all types of ambiguities, trivial or nontrivial. The close relevant to this work is considered in [7], where $3n_1n_2$ measurements are measured in the form of $M(u)$ (1.1), and PR's uniqueness holds if $s_1, s_2$ in (1.2) are integers. The result is included here.

THEOREM 2.1. *[7, Theorem 3.3] Assume that the DFT of $u \in \mathbb{C}^{n_1 \times n_2}$ is non-vanishing (each component is nonzero). Then $u$ can be recovered up to global phase (unique up to a multiplication with a unit scalar) from $3n_1n_2$ measurements in* (1.1)*, if and only if $s_i$ is prime with $n_i (i = 1, 2)$ and $n_1$ is prime with $n_2$.*

Due to the nonconvex nature of PR, numerical algorithms are often stuck at the local minimizers. Consequently it is not surprising that $3n_1n_2$ is empirically insufficient to give a satisfactory reconstruction, and one remedy suggested in [7] is via over-sampling. We find that $3n_1n_2$ measurements are sufficient if $s_1 = s_2 = 1/2$, as opposed to integers in [7], with additional assumption that the underlying image $u$ is real-valued and non-negative. Please refer to Section 5.1 for numerical validation of $s_1 = s_2 = 1/2$ and comparison to integer values. The theoretical guarantee is given in the following theorem.

THEOREM 2.2. *Assume that $u$ is non-negative and real-valued, the DFTs of $u$ and $D^s u$ are non-vanishing, and $s_1 = s_2 = 1/2$. Then $u$ can be recovered from $3n_1n_2$ measurements in* (1.1)*, if $n_1$ is prime with $n_2$.*

*Proof.* This theorem holds for both 1-D and 2-D cases. Here we only give a sketch proof for 1-D case, and see the complete proof in the Appendix.

In 1-D cases, $u = (u_0, u_1, \ldots, u_{n-1})^T \in \mathbb{R}^n$, and $u_k \geq 0, \forall 0 \leq k \leq n-1$. Since $u$ is real-valued and $\mathcal{F}u$ is non-vanishing, one has

$$U_{\mod (n-k,n)} = \bar{U}_k \neq 0, \quad \forall 0 \leq k \leq n-1, \tag{2.1}$$

where $U = (U_0, U_1, \ldots, U_{n-1})^T := \mathscr{F}u$, $\bar{z}$ denotes the complex conjugate of $z$. Similarly, one readily has

$$V_{\mod (n+1-k,n)} = \bar{V}_k \neq 0, \forall 0 \leq k \leq n-1, \tag{2.2}$$

where $V = (V_0, V_1, \ldots, V_{n-1})^T := \mathscr{F}D^s u$.

In the following we will study how to solve $U$ and $V$ alternatively by the relations in (2.1) and (2.2). As the triple $(|U_0|, |U_0 + V_0|, |U_0 - \mathbf{i}V_0|)$ is known, and $U_0$ is nonnegative real-valued, we can solve $U_0, V_0$ if $U_0 \neq 0, V_0 \neq 0$. We will use (2.1) and (2.2) to find the next triple, which can be solved as the similar manner of the previous one. One can readily find another triple $(|\bar{U}_1|, |\bar{U}_1 + \bar{V}_0|, |\bar{U}_1 - \mathbf{i}\bar{V}_0|)$ as the next one, and we can also obtain $U_1$ if $U_1 \neq 0$. Repeatedly, one can sequentially obtain all the $\{U_i\}_{i=0}^{n-1}$ and $\{V_i\}_{i=0}^{n-1}$. That finishes the proof in the 1-D case by inverse Fourier transformation of $U$. □

Although Theorem 2.2 has a similar statement to Theorem 3.3 in [7], the proof is different (cf. Appendix), as we exploit the nonnegativity of the original image $u$, and $s_1 = s_2 = 1/2$ is heuristically prime to $n_1, n_2$. More importantly, not only does the choice of $s_1 = s_2 = 1/2$ empirically yields exact recovery when using full (3 sets) data, but it also enables phase retrieval with significant amount of downsampling and noise in the measurement data. Note that non-vanishing DFT condition is mild, since one can use masks to scramble the Fourier transform to make it non-zero [7] (we do not consider this mask in experiments). To this end, we study the image reconstruction problem from the incomplete noisy measurements of $M(u)$, *i.e.*, downsampling the data by random binary masks, with additive Gaussian noise.

REMARK 2.1. *One can consider a more general problem as*

$$\text{find } u, \quad s.t. \;\; b := \mathcal{M}(u) = |\mathcal{L}u|, \tag{2.3}$$

*where $\mathcal{M}$ is a nonlinear mapping, specifically taking magnitudes of a linear transformation $\mathcal{L}$ on the signal $u$. Phase retrieval is a special case of* (2.3)*, as $\mathcal{L}$ is a subsampling of the Fourier matrix. The injectivity of $\mathcal{M}$ (the uniqueness) does not hold from Fourier measurements due to trivial ambiguities, such as the positivity, compact support for real-valued $u$. In [26], at least $2^d$ times measurements by oversampling are needed to obtain the injectivity theoretically for $d-$dimensions real-valued problems. For the general phase retrieval problems, the injectivity is guaranteed by collecting $K \geq 2N - 1$ [1] and $K \geq 4N - 4$ [13] measurements for real $u \in \mathbb{R}^N$ and complex $u \in \mathbb{C}^N$ signals respectively, provided that all mapping $\mathcal{M}$ generated by a generic frame*[2]*. In particular, Shechtman et al. [41] showed that the lower bound $2N - 1$ can be achieved with high probability by collecting full-spark random measurements, following the work [1]. By collecting $3N$ non-random Fourier measurements generated by deterministic masks for $u \in \mathcal{C}^N$, the uniqueness is derived in [7].*

*As stated in [31, 7], the theory of injectivity or the uniqueness in the afore mentioned work could not tell us how to retrieve the phases from the clean and noisy data, and one can not readily translate the theoretical results to the numerical simulation and practical applications. For example, it is proved in [7] that $3N$ measurements with integer $s$ can guarantee the uniqueness of the solution, but empirically at least $7N$ measurements for 1D case are needed to yield reasonable results. We added Figure 4 to show that at least $7N$ measurements for 2D case ($N = n_1 \times n_2$) for integer-valued $s$ yield worse results in terms of SNR compared to $3N$ measurements with $s_i = 1/2$.*

**3. Proposed models.** To account for down-sampling, we introduce three subsets: $\Omega_i \subset \Omega$, for $0 \leq i \leq 2$, each of which provides a binary mask of the incomplete FT

[2]Generic frame means a $K-$element frame belongs to an open dense subset of the set of all $K-$element frames in $\mathbb{R}^n$ or $\mathbb{C}^n$ [1]

magnitude. Then phase retrieval from the partial FT magnitudes can be formulated as a least-square type of minimization with a box constraint,

$$\min_{0\le u\le 1} \||\mathscr{F}u| - b_0\|_{\Omega_0}^2 + \||\mathscr{F}(u + D^s u)| - b_1\|_{\Omega_1}^2 + \||\mathscr{F}(u - \mathbf{i}D^s u)| - b_2\|_{\Omega_2}^2, \tag{3.1}$$

where $\|v\|_S := (\sum_{j\in S} |v(j)|^2)^{\frac{1}{2}}$ for $S \subset \Omega$. To simplify, we introduce a linear operator $\mathscr{A} := [\mathcal{I}, \mathcal{I} + D^s, \mathcal{I} - \mathbf{i}D^s]^T$, where $\mathcal{I}$ is the identity operator; and hence $\mathscr{A}u = (u, u + D^s u, u - \mathbf{i}D^s u)$. Denote $b := (b_0, b_1, b_2)$, $\bar{\Omega} := (\Omega_0, \Omega_1, \Omega_2)$ and $\mathscr{F}z := (\mathscr{F}z_0, \mathscr{F}z_1, \mathscr{F}z_2)$ for $z = (z_0, z_1, z_2)$. Eqn. (3.1) is equivalent to

$$\min_{0\le u\le 1} \mathscr{E}_{LSB} = \||\mathscr{F}\mathscr{A}u| - b\|_{\bar{\Omega}}^2, \tag{3.2}$$

which is referred to as least-square box (LSB) model. The LSB model yields an exact recovery if complete information ($3n_1n_2$ measurements) is available. With extreme downsampling, *e.g.* using only $10\% \times 3n_1n_2$ measurements, the reconstructed result of LSB contains visible artifacts, as illustrated in Figure 1 (c).

To further improve the results, we incorporate a total variation (TV) regularization [39] into (3.2), referred to as TVB model,

$$\min_{0\le u\le 1} \mathscr{E}_{TVB}(u) = \mathrm{TV}(u) + \frac{\lambda}{2}\||\mathscr{F}\mathscr{A}u| - b\|_{\bar{\Omega}}^2, \tag{3.3}$$

where $TV(u)$ denotes the discrete total variation semi-norm, i.e., the $L^1$ norm of the discrete gradient of $u$, and the parameter $\lambda$ balances the regularization term and the data fitting term. The objective functional favors the solution being approximately piecewise constant, and the model is effective for the data which is corrupted by the Gaussian white noise, i.e. $\hat{b}_i = b_i + \sigma n_i$, where $n_i \sim N(0,1)$ and $\sigma$ is the standard deviation. Other types of noise can be processed by changing the data fitting terms, which is beyond the scope of our paper. One can readily infer from Figure 1 (d) that TV regularization significantly improves the LBS.

We prove the existence of minimizer to the TVB model (3.3) in the continuous setting, which holds in the discrete case. Denote $\Omega$ be the bounded and Lipschitz-regular domain, and we obtain the existence of the minimizer.

THEOREM 3.1. *Given non-negative real data $b = (b_0, b_1, b_2)$, the TVB model* (3.3) *has at least one minimizer $u^* \in BV(\Omega)$.*

*Proof.* One readily knows $\mathscr{E}_{TVB}(u) \ge 0$. Hence, there exists a minimizing sequence $\{u_k\}_{0\le k\le\infty}$, s.t. $\mathscr{E}_{TVB}(u_0) \ge \mathscr{E}_{TVB}(u_1) \ge \ldots$. As $0 \le u_k \le 1$ and $\Omega$ is bounded and Lipschitz-regular, there exists a positive constant $C$, s.t. $\mathrm{TV}(u_k) + \|u_k\|_1 \le C$. By Rellich's compactness theorem, there exists $u^* \in BV(\Omega)$, and subsequence $(u_{n_k})_{k\ge1}$, such that $u_{n_k} \to u^*$ in $L^1(\Omega)$ as $k$ tends to $+\infty$. By the continuity of the second term of $\mathscr{E}_{TVB}$ and TV's lower semi-continuity, one obtains

$$\limsup_{u_{n_k}\to u^*} \mathscr{E}_{TVB}(u_k) \ge \mathscr{E}_{TVB}(u^*).$$

Therefore, $u^*$ is one minimizer of $\mathscr{E}_{TVB}(u)$. □

## 4. Numerical Algorithms.

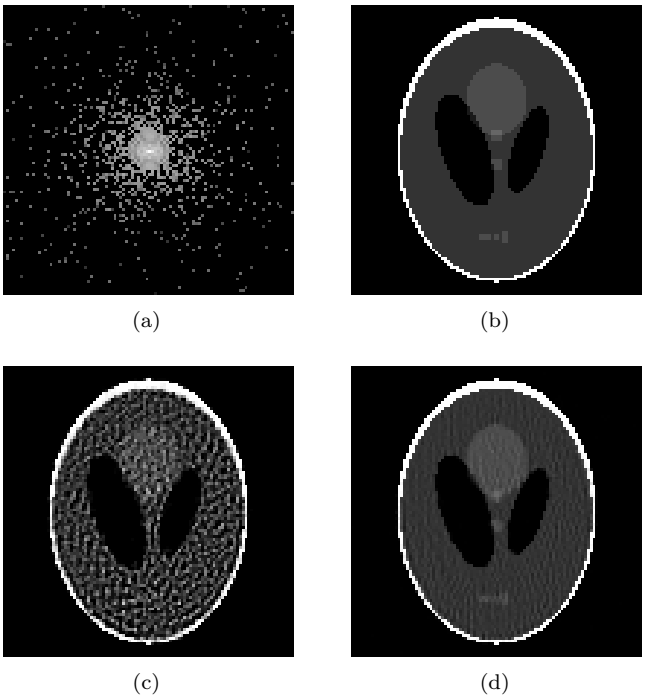

(a) (b)

(c) (d)

FIG. 1. *(a): 10% mask; (b): Original image (Resolution:* $100 \times 100$*); (c): phase retrieval by LSB with SNR=8.65; (d): phase retrieval by TVB with SNR=22.47.*

**4.1. Solving the LSB model.** There are numerious algorithms available to solve the LSB model (3.2), such as the error reduction (ER) [22], hybrid input-output (HIO) [19], hybrid projection-reflection (HPR) [15, 3] *etc.* It is studied in [44] that ADMM outperforms these projection algorithms (ER, HIO and HPR) in terms of both image quality and convergence rates, and hence we adopt ADMM here. As ADMM is a first-order algorithm [27] for non-differential convex optimization problems, we will explore fast algorithms in the future, such as [4] with second-order convergence rate and parallel acceleration [11]. The LSB model (3.2) can be rewritten as

$$\begin{aligned} &\min_u \frac{1}{2}\||z| - b\|_\Omega^2 + \chi(v), \\ &s.t. \quad \begin{cases} u = v, \\ z = \mathscr{F}\mathscr{A}u, \end{cases} \end{aligned}$$

where $z = (z_0, z_1, z_2)$, and

$$\chi(v) = \begin{cases} 0, & 0 \le v \le 1; \\ \infty, & \text{otherwise.} \end{cases}$$

The augmented Lagrangian reads

$$\begin{aligned} \mathscr{L}_{LSB}(u, v, z; w, d) = &\frac{1}{2}\||z| - b\|_\Omega^2 + \chi(v) + \Re\langle d, z - \mathscr{F}\mathscr{A}u\rangle \\ &+ \frac{\rho_1}{2}\|z - \mathscr{F}\mathscr{A}u\|^2 + \langle w, u - v\rangle + \frac{\rho_2}{2}\|u - v\|^2, \end{aligned} \tag{4.1}$$

where $d = (d_0, d_1, d_2)$ and $\rho_1, \rho_2$ are positive parameters. The ADMM for this saddle point problem involves minimizing $\mathscr{L}_{LSB}$ with respect to $u, v, z$ alternatively while updating the dual variables $d$ and $w$. The algorithm is summarized in Algorithm 1.

Below we elaborate on how to solve these three subproblems,

$$u^{k+1} = \arg\min_u \mathscr{L}_{LSB}(u, v^k, z^k; w^k, d^k), \tag{4.2}$$

$$v^{k+1} = \arg\min_v \mathscr{L}_{LSB}(u^{k+1}, v, z^k; w^k, d^k), \tag{4.3}$$

$$z^{k+1} = \arg\min_z \mathscr{L}_{LSB}(u^{k+1}, v^{k+1}, z; w^k, d^k). \tag{4.4}$$

There are closed-form solutions for (4.3) and (4.4). The expression for $v$ is given by

$$v^{k+1} = \min\left\{1, \max\left\{0, u^{k+1} + w^k/\rho_2\right\}\right\}. \tag{4.5}$$

Minimization for each component of $z$ is independent of other two, so we just describe how to solve for $z_0$ as an example. The solution of

$$\min_{z_0} \frac{1}{2\rho_1}\||z_0| - b_0\|^2_{\Omega_0} + \frac{1}{2}\|z_0 + d_0/\rho_1 - \mathscr{F}u\|^2,$$

can be expressed as

$$z_0^* = \begin{cases} \dfrac{b_0 + \rho_1|g_0|}{1+\rho_1}\dfrac{g_0}{|g_0|}, & \text{if } x \in \Omega_0 \cap \{g_0 \neq 0\}; \\ \dfrac{b_0}{1+\rho_1}c^*, & \text{if } x \in \Omega_0 \cap \{g_0 = 0\}; \\ g_0, & \text{otherwise.} \end{cases} \tag{4.6}$$

where $g_0 = \mathscr{F}u - d_0/\rho_1$, $\forall c^* \in \mathbb{C}$ with $|c^*| = 1$. To minimize $\mathscr{L}_{LSB}$ with respect to $u$, we calculate the derivatives

$$\partial_u\left(\|z_0 - \mathscr{F}u\|^2/2\right) = \partial_u\left(\|\mathscr{F}^*z_0 - u\|^2/2\right) = u - \Re(\mathscr{F}^*z_0), \tag{4.7}$$

$$\partial_u\left(\|z_1 - \mathscr{F}(u + D^s u)\|^2/2\right) = (2 + 2\Re(D^s))u - \Re(\mathscr{F}^*z_1 + D^s\overline{\mathscr{F}^*z_1}\ ), \tag{4.8}$$

$$\partial_u\left(\|z_2 - \mathscr{F}(u - \mathbf{i}D^s u)\|^2/2\right) = (2 + 2\Im(D^s))u - \Re(\mathscr{F}^*z_2 - \mathbf{i}D^s\overline{\mathscr{F}^*z_2}\ ), \tag{4.9}$$

where $\mathscr{F}^*$ denotes the inverse Fourier transform, $\bar{z}$ denotes the complex conjugate of $z$. Therefore, (4.2) is equivalent to solving $u$ from

$$\begin{aligned} &\left(\rho_1(5 + 2\Re(D^s) + 2\Im(D^s)) + \rho_2\mathcal{I}\right)u \\ &= \rho_1(\Re(\hat{z}_0^k + \hat{z}_1^k + D^s\bar{\hat{z}}_1^k + \hat{z}_2^k) + \Im(D^s\bar{\hat{z}}_2^k)) + (\rho_2 v^k - w^k), \end{aligned} \tag{4.10}$$

where $\hat{z}_i^k = \mathscr{F}^*(z_i^k + d_i^k/\rho_1)$ for $0 \le i \le 2$. Note that each diagonal element of $D^s$ is a complex number with magnitude not greater than 1 , and hence $5\mathcal{I}+2\Re(D^s)+2\Im(D^s)$ is invertible, and (4.10) can be solved efficiently by direct inversion of the diagonal matrix $\rho_1(5\mathcal{I} + 2\Re(D^s) + 2\Im(D^s)) + \rho_2\mathcal{I}$, *i.e.*,

$$\begin{aligned} u = &\left(\rho_1(5 + 2\Re(D^s) + 2\Im(D^s)) + \rho_2\mathcal{I}\right)^{-1} \times \\ &\left(\rho_1(\Re(\hat{z}_0^k + \hat{z}_1^k + D^s\bar{\hat{z}}_1^k + \hat{z}_2^k) + \Im(D^s\bar{\hat{z}}_2^k)) + (\rho_2 v^k - w^k)\right). \end{aligned} \tag{4.11}$$

**Algorithm 1** ADMM for solving the LSB model (3.2)

Initialization. $k=0, w^0=0, d^0=0, v^0, z^0$.
**while** stopping conditions are not satisfied **do**
Solve (4.10) via (4.11) to obtain $u^{k+1}$;
Update $v^{k+1}$ via (4.5);
Update $z_0^{k+1}$ via (4.6), similarly for $z_1^{k+1}, z_2^{k+1}$;
Update the dual variables

$$\begin{cases} d^{k+1} = d^k + \rho_1(z^{k+1} - \mathscr{F}\mathscr{A}u^{k+1}), \\ w^{k+1} = w^k + \rho_2(u^{k+1} - v^{k+1}); \end{cases} \tag{4.12}$$

$k \leftarrow k+1$.
**end while**
output the solution $u^* = u^{k+1}$.

**4.2. Solving the TVB model** (3.3)**.** Inspired by split Bregman [24] or equivalently ADMM, we introduce an auxiliary variation $\boldsymbol{p}$ and rewrite (3.3) as

$$\begin{aligned} \min_u \mathscr{E}_{TVB}(u) &:= \|\boldsymbol{p}\|_1 + \frac{\lambda}{2}\||z|-b\|^2_{\Omega_0,\Omega_1,\Omega_2} + \chi(v), \\ \text{s.t.} \quad & u = v, \quad \boldsymbol{p} = \nabla u, \quad z = \mathscr{F}\mathscr{A}u. \end{aligned} \tag{4.13}$$

The augmented Lagrangian of $\mathscr{E}_{TVB}(u)$ reads

$$\begin{aligned} &\mathscr{L}_{TVB}(u, v, \boldsymbol{p}, z; w, \boldsymbol{q}, d) \\ = \quad & \|\boldsymbol{p}\|_1 + \frac{\lambda}{2}\||z|-b\|^2_{\Omega_0,\Omega_1,\Omega_2} + \chi(v) + \Re\langle d, z - \mathscr{F}\mathscr{A}u\rangle + \frac{\rho_1}{2}\|z - \mathscr{F}\mathscr{A}u\|^2 \\ & + \langle \boldsymbol{q}, \boldsymbol{p} - \nabla u\rangle + \langle w, u - v\rangle + \frac{\rho_2}{2}\|u-v\|^2 + \frac{\rho_3}{2}\|\boldsymbol{p} - \nabla u\|^2, \end{aligned} \tag{4.14}$$

where $\boldsymbol{q}: \Omega \to \mathbb{R}^2$ and $\rho_1$, $\rho_2$, $\rho_3$ are positive parameters. Again we apply ADMM to solve the saddle point problem

$$\max_{w,\boldsymbol{q},d} \quad \min_{u,v,\boldsymbol{p},z} \mathscr{L}_{TVB}(u, v, \boldsymbol{p}, z; w, \boldsymbol{q}, d).$$

Please refer to Algorithm 2. Below we only describe the difference to Algorithm 1 in details.

The subproblem to minimize over $u$ is simplified by omitting superscripts and subscripts,

$$\min_u \quad \frac{1}{2}\|\boldsymbol{p} + \boldsymbol{q}/\rho_3 - \nabla u\|^2 + \frac{\rho_2}{2\rho_3}\|u - v + w/\rho_2\|^2 + \frac{\rho_1}{2\rho_3}\Big(\|z + d/\rho_1 - \mathscr{F}\mathscr{A}u\|^2\Big). \tag{4.15}$$

By calculating the derivative,

$$\partial_u\left(\|\boldsymbol{p} + \boldsymbol{q}/\rho_3 - \nabla u\|^2/2\right) = \operatorname{div}(\boldsymbol{p} + \boldsymbol{q}/\rho_3 - \nabla u) = -\Delta u + \operatorname{div}(\boldsymbol{p} + \boldsymbol{q}/\rho_3),$$

and together with (4.7)-(4.9), we can obtain the Euler-Lagrangian equation to (4.15)

$$\begin{aligned} & -\Delta u + \left(\frac{\rho_1}{\rho_3}(5 + 2\Re(D^s) + 2\Im(D^s)) + \frac{\rho_2}{\rho_3}\right) u \\ =& \frac{\rho_1}{\rho_3}(\Re(\hat{z}_0 + \hat{z}_1 + D^s\bar{\hat{z}}_1 + \hat{z}_2) + \Im(D^s\bar{\hat{z}}_2)) + \frac{1}{\rho_3}(\rho_2 v - w) - \operatorname{div}(\boldsymbol{p} + \boldsymbol{q}/\rho_3). \end{aligned}$$

**Algorithm 2** ADMM for solving the TVB model (3.3)

Initialization. $k=0, w^0=0, \boldsymbol{q}^0=0, d_i^0=0, v^0, z_i^0$.
**while** stopping conditions are not satisfied **do**
$u^{k+1}=\arg\min_u \mathscr{L}_{TVB}(u, v^k, \boldsymbol{p}^k, z^k; w^k, \boldsymbol{q}^k, d^k)$: solve for (4.16) via CG;
$v^{k+1}=\arg\min_v \mathscr{L}_{TVB}(u^{k+1}, v, \boldsymbol{p}^k, z^k; w^k, \boldsymbol{q}^k, d^k)$: similar to (4.5);
$\boldsymbol{p}^{k+1}=\arg\min_{\boldsymbol{p}} \mathscr{L}_{TVB}(u^{k+1}, v^{k+1}, \boldsymbol{p}, z^k; w^k, \boldsymbol{q}^k, d^k)$: see (4.17);
$z^{k+1}=\arg\min_z \mathscr{L}_{TVB}(u^{k+1}, v^{k+1}, \boldsymbol{p}^{k+1}, z; w^k, \boldsymbol{q}^k, d^k)$: similar to (4.6);
Update dual variables

$$\begin{cases} d^{k+1}=d^k+\rho_1(z^{k+1}-\mathscr{F}\mathscr{A}u^{k+1}), \\ w^{k+1}=w^k+\rho_2(u^{k+1}-v^{k+1}), \\ \boldsymbol{q}^{k+1}=\boldsymbol{q}^k+\rho_3(\boldsymbol{p}^{k+1}-\nabla u^{k+1}), \end{cases} \tag{4.18}$$

$k\leftarrow k+1$.
**end while**
output the solution $u^*=u^{k+1}$.

where $\hat{z}_i=\mathscr{F}^*(z_i+d_i/\rho_1)$ for $0\le i\le 2$. This equation is a linear second order PDE as $-\Delta u+\frac{\rho_1}{\rho_3}au=f$, for $a(x_1,x_2)=5+2\Re(D^s)+2\Im(D^s)+\frac{\rho_2}{\rho_1}\ge 1+\frac{\rho_2}{\rho_1}$, which can be solved efficiently. In particular, we adopt the five-point difference discretization scheme, and solve the following equation to obtain $u^{k+1}$ via conjugate gradient (CG) method,

$$\begin{aligned} &-\Delta u+\left(\frac{\rho_1}{\rho_3}(5+2\Re(D^s)+2\Im(D^s))+\frac{\rho_2}{\rho_3}\right)u \\ =&\frac{\rho_1}{\rho_3}(\Re(\hat{z}_0^k+\hat{z}_1^k+D^s\bar{\hat{z}}_1^k+\hat{z}_2^k)+\Im(D^s\bar{\hat{z}}_2^k))+\frac{1}{\rho_3}(\rho_2 v^k-w^k)-\operatorname{div}(\boldsymbol{p}^k+\boldsymbol{q}^k/\rho_3), \end{aligned} \tag{4.16}$$

where $\hat{z}_i^k=\mathscr{F}^*(z_i^k+d_i^k/\rho_1)$ for $0\le i\le 2$. In addition, the update for $\boldsymbol{p}$ from

$$\min_{\boldsymbol{p}}\|\boldsymbol{p}\|_1+\frac{\rho_3}{2}\|\boldsymbol{p}+\boldsymbol{q}/\rho_3-\nabla u\|^2,$$

has a closed-form solution,

$$p=\text{Thresh}(-\boldsymbol{q}/\rho_3+\nabla u;1/\rho_3), \tag{4.17}$$

where the soft thresholding is denoted as $\text{Thresh}(\boldsymbol{p};\eta)=\boldsymbol{p}\max\left\{0,1-\frac{\eta}{\|\boldsymbol{p}\|}\right\}$.

**4.3. Convergence analysis.** We shall analyze whether the proposed algorithms converge. We only consider the convergence of TVB, as TVB reduces to LSB for sufficiently large $\lambda$. In order to deduce the KKT condition of (4.13), which is a real-valued objective functional with complex-valued constraints, one shall carefully deal with the derivatives, as this objective functional is not holomorphic with respect to the complex variables unless it is a constant. The $\mathbb{CR}$-calculus formalism [38, 28] is adopted to describe the derivatives. Assuming that the real-valued objective functional can be expressed as $\mathscr{D}(z,\bar{z})$ with respect to the variable $z$ and its conjugate $\bar{z}$, the first order

derivative can be defined as $\frac{\partial \mathscr{D}}{\partial z}$(or $\frac{\partial \mathscr{D}}{\partial \bar{z}}$ ). $z^*$ is a stationary point if $\frac{\partial \mathscr{D}(z^*,\bar{z}^*)}{\partial z} = 0$ or $\frac{\partial \mathscr{D}(z^*,\bar{z}^*)}{\partial \bar{z}} = 0$, and one can refer to [28] for details. Therefore, we can readily derive the KKT condition of (4.13) for some $u^*, v^*, \boldsymbol{p}^*, z^* = (z_0^*, z_1^*, z_2^*), w^*, \boldsymbol{q}^*, d^* = (d_0^*, d_1^*, d_2^*)$ (the first order condition of (4.14) without the augmented terms, i.e. $\rho_1 = \rho_3 = 0$)

$$\text{(KKT)} \qquad \begin{cases} 0 = -\Re(d_0^* + d_1^* + D^s\bar{d}_1^* + d_2^*) + \Im(D^s\bar{d}_2^*) + \operatorname{div}(\boldsymbol{q}^*) + w^*, \\ 0 \in \partial_{\boldsymbol{p}}\|\boldsymbol{p}^*\|_1 + \boldsymbol{q}^*, \\ 0 \in \lambda\partial_{z_i}|z_i^*| \cdot (|z_i^*| - b_0) + \dfrac{1}{2}\bar{d}_i^*, \ \forall 0 \le i \le 2, \\ 0 \ge \langle w^*, v - v^*\rangle, \forall 0 \le v \le 1, \\ 0 = u^* - v^*, \\ 0 = \boldsymbol{p}^* - \nabla u^*, \\ 0 = z^* - \mathscr{F}\mathscr{A}u^*. \end{cases}$$

THEOREM 4.1. *Let $(u^k, v^k, \boldsymbol{p}^k, z^k, w^k, \boldsymbol{q}^k, d^k)$ be generated by Algorithm 2. If the successive differences sequences of the multipliers $w^{k+1} - w^k, \boldsymbol{q}^{k+1} - \boldsymbol{q}^k, d^{k+1} - d^k$ all converge to 0 as k tends to $\infty$, then there exists a subsequence $S_{sub}$ whose accumulation point satisfies the KKT condition of* (4.13).

*Proof.* Define $X^k := (u^k, v^k, \boldsymbol{p}^k, z^k, w^k, \boldsymbol{q}^k, d^k)$. Since $\lim_{k\to 0}\left(d^{k+1} - d^k\right) = 0$, and the multiplier updates by (4.18), one readily obtains that

$$\lim_{k\to 0} z^k - \mathscr{F}\mathscr{A}u^k = 0. \tag{4.19}$$

As $0 \le v^k \le 1$, and $\lim_{k\to 0}\left(w^{k+1} - w^k\right) = 0$, there exists a bounded subsequence such that $\lim_{k\to\infty} u^k = \lim_{k\to\infty} v^k = u^*$ (still denoted as $u^k$, and $w^k$).

It follows from (4.6) and (4.19) that $\{d_0^k\}$ and $\{z_0^k\}$ are bounded, and similarly for $z_1^k, z_2^k, d_1^k, d_2^k$. The boundedness of $\boldsymbol{q}^k$ can be derived using the similar analysis in [44]. Therefore, there exists a bounded subsequence $\{X^{n_k}\}$ converging to $X^* = \{u^*, v^*, \boldsymbol{p}^*, z^*, w^*, \boldsymbol{q}^*, d^*\}$. Then

$$\begin{cases} z^* = \mathscr{F}\mathscr{A}u^*, \\ \boldsymbol{p}^* = \nabla u^*, \end{cases}$$

The variational inequality of Step 2 in Algorithm 2 reads $\forall\ 0 \le v \le 1$,

$$\langle -w^k, v - v^{k+1}\rangle \ge -\rho_2\langle u^{k+1} - v^{k+1}, v - v^{k+1}\rangle \ge -\rho_2\|u^{k+1} - v^{k+1}\|\|v - v^{k+1}\|.$$

Hence

$$\langle -w^*, v - v^*\rangle \ge 0, \forall\ 0 \le v \le 1.$$

The proof for the first three relations in the KKT condition are similar to the ones in [44], which are omitted here. □

Note that the requirement of multipliers $w^{k+1} - w^k, \boldsymbol{q}^{k+1} - \boldsymbol{q}^k, d^{k+1} - d^k$ converging to zero in Theorem 4.1 seems rather strong, but it is common in nonconvex optimization, see [44, 46, 29]. The convergence rate for such nonconvex optimization problem will be considered as [27] in the future.

**5. Numerical examples.** The masks $\Omega_i$ are randomly generated, and we further assume that they are identical, *i.e.,* $\Omega_0 = \Omega_1 = \Omega_2$. Note that low DFT frequencies contain more signal over noise, while high frequencies contain the information determining the image resolution. As a result, the probability of selecting the lower frequencies data shall be higher than that of high frequencies if only measuring the partial magnitudes. Please refer to [33] for details about the different choice of the sampling masks. In this part, we use a random mask to generate $\Omega_0$ and produce the probability density function for 2D random sampling pattern with polynomial variable density sampling [32].

We consider random initialization for both LSB and TVB. Specifically, variables $v^0$ and $z_i^0$ are chosen to be

$$z_i^0(\omega) = \begin{cases} b_i(\omega)\exp(-2\pi \boldsymbol{i}\theta_i\omega), & \text{if } \omega \in \Omega, \\ 0, & \text{otherwise,} \end{cases}$$

and $v^0 = \mathscr{F}^* z_1^0$ where $\theta_i$ are drawn from the standard uniform distribution on the open interval (0,1). The gradient and divergence operators in the TVB model are discretized with the periodical boundary condition. We set the maximum iteration number to be 500. Relative-mean-squared-error (RMSE) and signal-noise-ratio (SNR) are used to measure the reconstruction quality

$$\mathrm{RMSE}(u, u_g) = \frac{\sum\limits_{j\in\Omega} |u(j) - u_g(j)|^2}{\sum\limits_{j\in\Omega} |u_g(j)|^2},$$

$$\mathrm{SNR}(u, u_g) = -10\log_{10}\mathrm{RMSE}(u, u_g),$$

where $u_g$ is the ground truth image of size $n_1 \times n_2$ and $u$ is the reconstructed image.

**5.1. Phase retrieval from complete information.** We first demonstrate the exact recovery theorem (Theorem 2.2) of phase retrieval using complete data $M(u)$ when $s_1 = s_2 = 1/2$. We employ the LSB model (3.1) on two testing cases: (1) 100 images that are randomly generated from uniform distribution on the interval $[0, 1] \times [0, 1]$; and (2) 50 natural images of resolutions $512 \times 512$ as shown in Figure 2. The SNR and RMSE values of the recovered images are put in Figure 3, which shows that RMSEs are in the order of $10^{-9}$ and $10^{-7}$ for the random data and natural images respectively, and SNRs are almost above 65dB and 40 dB for these two cases respectively (average SNRs are 87dB and 68dB respectively).

In addition, we find that the LSB model does not work well with $3N$ measurements if $s_1, s_2$ are chosen to be integers, which implies that the choice of $s_1 = s_2 = 1/2$ plays an important role in exact phase retrieval problem. For integer values $s_i$, Candés et al. [7] also suggested oversampling by using seven groups of data in order to give a stable recovery for 1-D case. We demonstrate that $7N$ measurements for integer-valued $s_i$ are even worse in Figure 4 than $3N$ measurements for $s_1 = s_2 = 1/2$. In particular, we consider 2-D real-valued images from Figure 2, and seven groups of data are adopted with $(s_1, s_2) = (0, 3), (3, 0)$, and $(5, 5)$. The SNR values are reported in Figure 4 with average value 29dB, which is much smaller than the case with average SNRs 68dB in Figure 3 (b).

We also compare our proposed ADMM with three related algorithms, ER (error reduction) algorithm [22], PhaseCut method [42], and Wirtinger flow (WTF) method [8]. We implement the ER by our own, which consists of the following three steps:

FIG. 2. *Natural images*

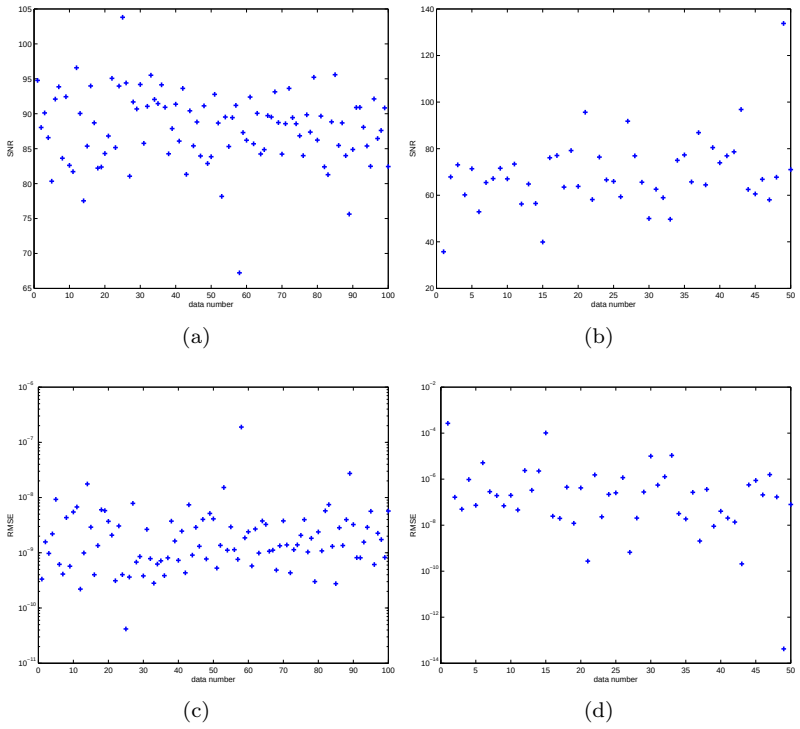


FIG. 3. *Exact recovery of complete information. (a) SNR values(dB) for random data with average value 87dB; (b) SNR values(dB) for natural images with average value 68dB; (c) Corresponding RMSE for random data; (d) Corresponding RMSE for natural images.*

Step 1. Initialize $u_0, z_0 := \mathscr{F}\mathscr{A}u_0$, which satisfies $|z_0| = b$ and set $k := 0$.
Step 2. Update $u$ by solving the following least square problem

$$\tilde{u} = \arg \min_{u \in \mathbb{R}^{n_1 \times n_2}} \|\mathscr{F}\mathscr{A}u - \tilde{z}\|^2,$$

where $\tilde{z}(t) = b(t)z_k(t)/|z_k(t)|,\ 0 \le t \le n_1 n_2 - 1.$

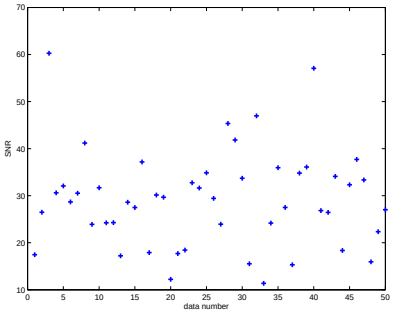


FIG. 4. *Exact recovery of complete information with seven groups of data with* $(s_1, s_2) = (0, 3), (3, 0)$, *and* $(5, 5)$*: SNR values(dB) for natural images with average value 29dB. Obviously the recovery qualities by using seven groups of data by setting* $s_i$ *as integers are much worse than those by setting* $s_i = 1/2$ *in Fig. 3 (b) with average SNRs 68dB.*

Step 3. Update $u_{k+1}$ by a simple projection as

$$u_{k+1} = \min\{\max\{\tilde{u}, 0\}, 1\}$$

and $z_{k+1} = \mathscr{F}\mathscr{A}u_{k+1}$. If satisfying some stopping condition, then stop and output $u_{k+1}$ as the final result; Otherwise, set $k := k + 1$ and goto Step 2.

We use the source codes of PhaseCut[3] [42] to solve for the LSB model, with further refinement by ER algorithm to obtain final results, similar to [21]. We adopt the WTF scheme to our problem, which requires the solution to be real-valued with box constraint. In particular, we use an iterative scheme to solve

$$\min_{0\le u\le 1} G(u) := \left\| |\mathscr{F}\mathscr{A}u|^2 - b^2 \right\|^2,$$

by using a gradient projection method with adaptive steps

$$u^{k+1} = \max\{0, \min\{1, \hat{u}^{k+1}\}\}, \text{with } \hat{u}^{k+1} = u^k - \tau^k \nabla_u G(u^k), \quad k = 0, 1, \cdots$$

where $\tau^k$ is the adaptive step. It seems that for LSB model the step-selecting scheme for $\tau^k$ proposed in the numerical experiment of [8] does not work well. We further apply backtracking search technique [4] and consider two initialization schemes: random and spectral initialization.

The comparison results to ER algorithm, WTF method, and PhaseCut are illustrated in Figure 5, which show that our proposed ADMM for LSB model are more robust and efficient than these two other algorithms. For possible improvement of the numerical performance for Wirtinger flow method, we will investigate how to develop a more effective optimization model with different objective functional, where a good initialization and more efficient numerical optimization schemes should be provided meanwhile. In addition, a future work is how to reduce the computation complexity for LSB model considering that the result in Figure 5 (d) generated by PhaseCut is reasonably good.

[3]Available at http://www.di.ens.fr/ aspremon/PhaseCutCode

(a) ER (b) WTF+random (c) WTF+spectral

(d) PhaseCut (e) Ours

FIG. 5. *Results for LSB model by ER algorithm (stopped after 5000 iterations) in (a) with SNR=15.81, WTF in (b) with SNR=10.45 with random initialization, WTF in (c) with SNR=13.66 with spectral initialization, PhaseCut method (refinement by ER method as [21]) in (d) with SNR=19.27, and ADMM in (e) with SNR=53.91. Here we used the backtracking technique to improve WTF [8].*

**5.2. Noiseless incomplete measurements.** We demonstrate the performance of both LSB and TVB models when limited measurements are available. The parameters for the TVB model are put in Table 1, and we set the parameters $\rho_1 = 0.001$ and $\rho_2 = 0.01$ for the LSB for all the testing cases. The numerical results are presented in Figures 6-8, which show that the LSB model produces more visible artifacts than the TVB. With TV regularization, the image qualities are significantly improved with an average increase of 4db in SNR values. We present the reconstructed images at different iteration numbers in Figure 9, which illustrates how the method gradually recovers the image and converges after hundreds of iterations. Figure 10 plots energy and relative errors with respect to the iteration, which numerically verifies the convergence analysis (Theorem 4.1).

All the tests are performed on a desktop computer with Intel(R) Core(TM) i3-2310 CPU@3.30GHz and 4.00GB RAM. The computational time is recorded in Table 2, which shows that TVB is slower than LSB due to an additional sparse linear system to solve. Computationally, the conjugate gradient method(CG) is adopted to solve the linear system, and it is found that a few CG iterations are sufficient to give satisfactory results.

**5.3. Noisy incomplete measurements.** Now we consider both incomplete and noisy measurements. The data are corrupted by the white Gaussian noise, *i.e.*, $\hat{b}_i = b_i + \sigma n_i$, where $\sigma$ is the noisy level, and $n_i$ denotes the white Gaussian noise

| Figures | $\lambda$ | $\rho_1$ | $\rho_2$ | $\rho_3$ |
|---|---|---|---|---|
| Figure 6 (d) | 1000 | 0.1 | 0.1 | 0.02 |
| Figure 6 (g) | 1000 | 0.4 | 0.2 | 0.02 |
| Figure 7 (d) | 100 | 0.07 | 0.08 | 0.02 |
| Figure 7 (g) | 1000 | 0.1 | 0.1 | 0.02 |
| Figure 8 (d) | 1000 | 0.08 | 1 | 0.02 |
| Figure 8 (g) | 1000 | 0.2 | 1 | 0.02 |

TABLE 1
*Parameters for Algorithm 2*

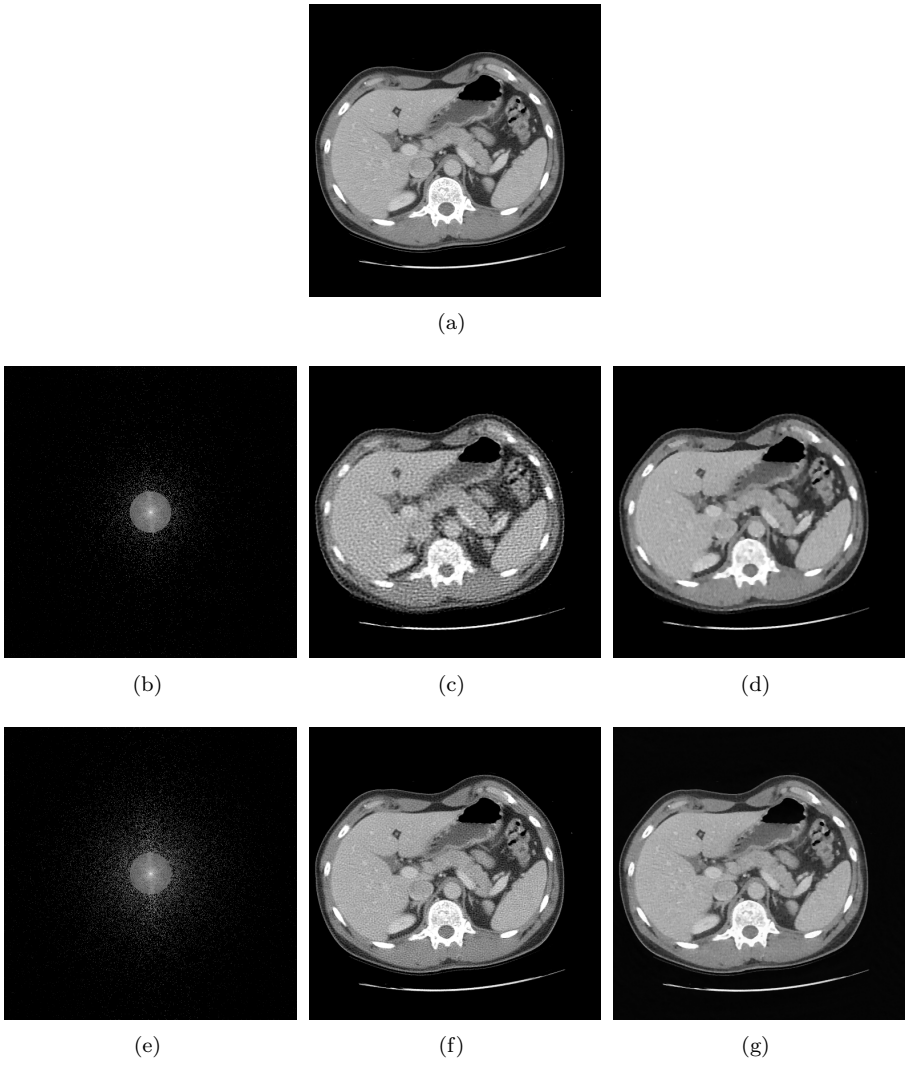

FIG. 6. *(a): Original image (Resolution:* $512 \times 512$*); (b):* 5% *mask; (c): phase retrieval by LSB with SNR=16.42; (d): phase retrieval by TVB with SNR=20.77; (e):* 10% *mask; (f): phase retrieval by LSB with SNR=18.86; (g): phase retrieval by TVB with SNR=23.95.*

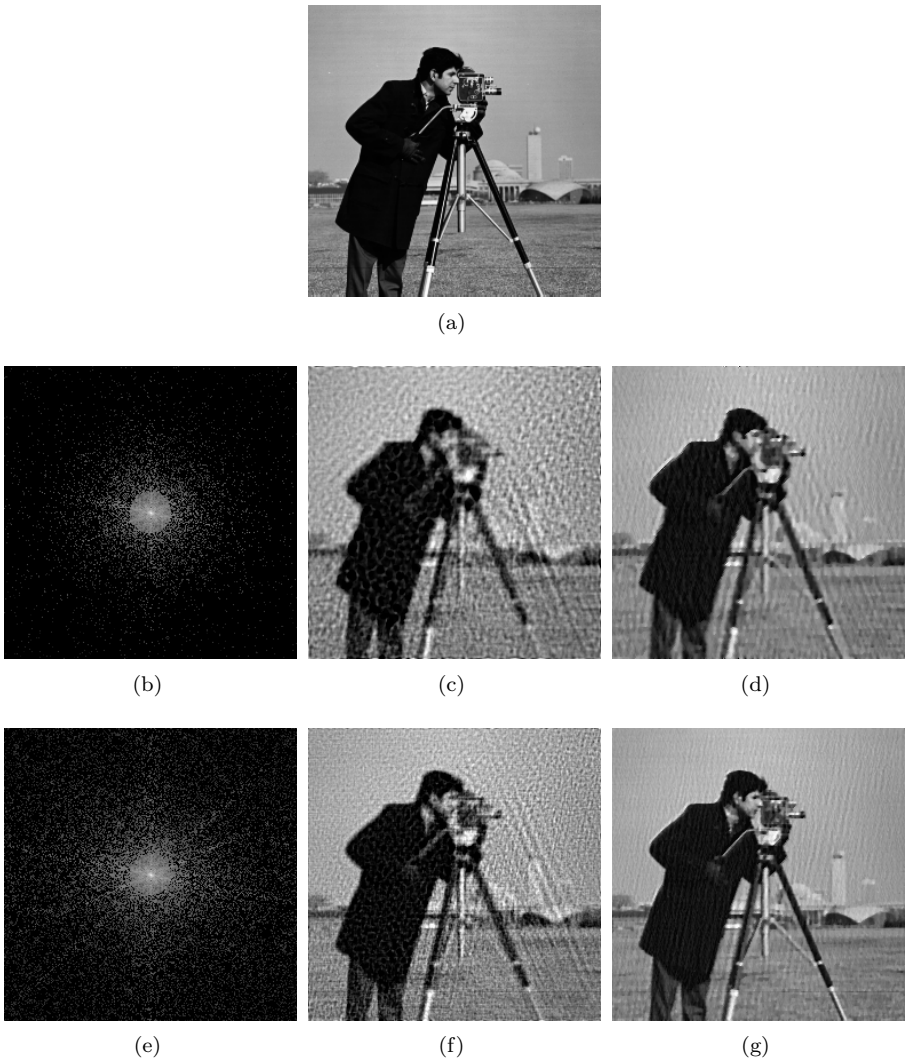

(a)

(b) (c) (d)

(e) (f) (g)

FIG. 7. *(a): Original image (Resolution:* $256 \times 256$*); (b):* 10% *mask; (c): phase retrieval by LSB with SNR=14.50; (d): phase retrieval by TVB with SNR=18.04; (e):* 30% *mask; (f): phase retrieval with LSB, SNR=15.35; (g): phase retrieval by TVB with SNR=19.29.*

| Name | pixels | Mask(ratio) | time (s) of LSB | time (s) of TVB |
|---|---|---|---|---|
| Leaf | $256 \times 256$ | 10% | 29.36 | 36.54 |
| Leaf | $256 \times 256$ | 30% | 28.15 | 37.03 |
| Cameraman | $256 \times 256$ | 10% | 27.82 | 37.18 |
| Cameraman | $256 \times 256$ | 30% | 28.59 | 37.98 |
| Liver | $512 \times 512$ | 5% | 132.2 | 178.8 |
| Liver | $512 \times 512$ | 10% | 132.8 | 179.7 |

TABLE 2
*Elapsed time for LSB and TVB.*

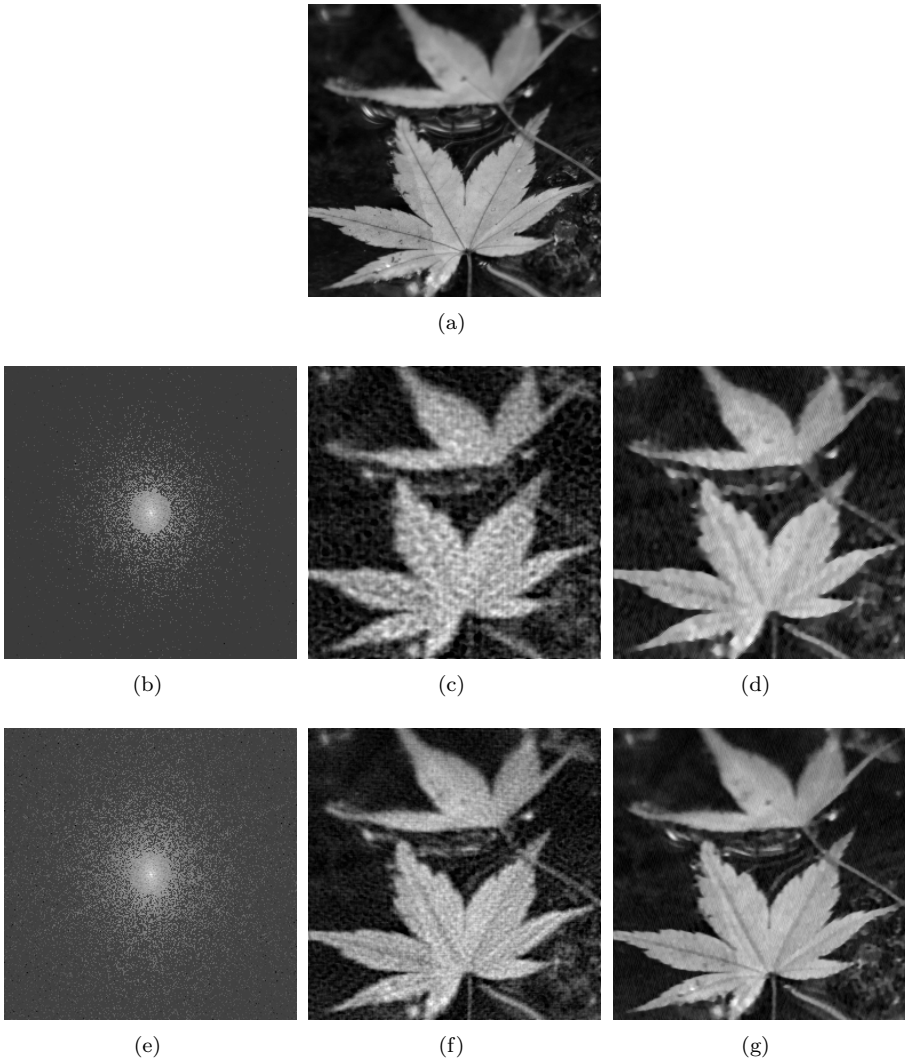

(a)

(b) (c) (d)

(e) (f) (g)

FIG. 8. *(a): Original image "Leaf" (Resolution:* $256\times256$*); (b):* 10% *mask; (c): phase retrieval by LSB with SNR=14.19; (d): phase retrieval by TVB with SNR=18.35; (e):* 30% *mask; (f): phase retrieval by LSB with SNR=17.41; (g): phase retrieval by TVB with SNR=22.75.*

with the zero mean. The SNR of the noisy measurements is defined as

$$\mathrm{SNR}(N,M) = -10\log_{10}\big(\sum_{j\in\Omega_0,0\le k\le 2}|\hat{b}_k(j)-b_k(j)|^2/\sum_{j\in\Omega_0,0\le k\le 2}|b_k(j)|^2\big),$$

where $N=\{\hat{b}_0,\hat{b}_1,\hat{b}_2\}$ is the noisy measurement with respect to the mask $\Omega_0$, and $M=\{b_0,b_1,b_2\}$ is the ground truth measurement. Therefore, noise level $\sigma$ can be determined by the SNR value, *i.e.*,

$$\sigma=\sqrt{\frac{10^{-\mathrm{SNR}/10}\sum\limits_{0\le k\le 2,j\in\Omega_0}|b_k(j)|^2}{3d}},$$

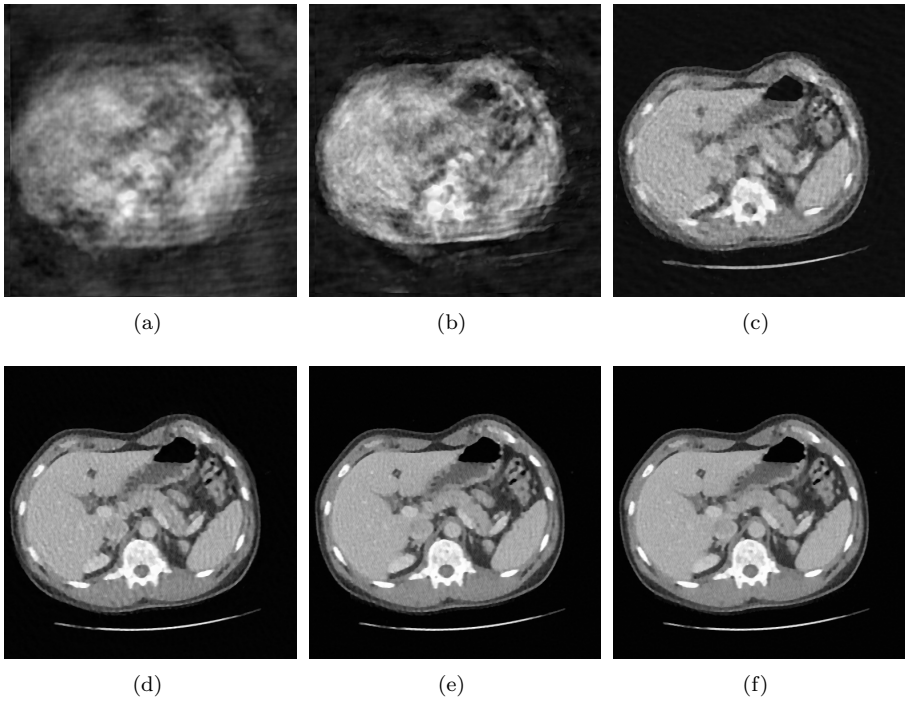

FIG. 9. *(a): SNR=6.47 after 10 iterations; (b): SNR=9.48 after 30 iterations; (c): SNR=14.89 after 100 iterations; (d): SNR=18.33 after 200 iterations; (e): SNR=19.95 after 300 iterations; (f): SNR=20.15 after 400 iterations*

where $d = \#\{j : j \in \Omega_0\}$. The parameters for the TVB are set to be $\lambda = 1000, \rho_1 = 0.1, \rho_2 = 0.1, \rho_3 = 0.02$ for both Figure 11 (d) and Figure 11 (f). The SNR values of the TVB are increased at least 4db compared to the LSB.

**5.4. Initialization and Parameters sensitivity.** As is know, the proposed model is not convex, thus sensitive to initialization and model parameters. We analyze the effects of random initialization, i.e., random $\theta_i$, when applying the proposed method on "Cameraman" image with a 30% mask. Figure 12 (a) shows that the SNR values of restored images vary from 18.4dB to 19.8dB, which suggests that the proposed algorithm is rather robust to initialization. By comparing Figure 12 (b) with Figure 7 (g), we find that averaging the reconstructed images with different initializations yields better image quality than individual ones, which is a trick suggested by Fienup and Wackerman [20] to remove artifacts.

In addition, we shall study whether the proposed algorithm is sensitive to parameters, by varying one parameter and fixing the others. The default parameters are set to be the same as Figure 7 (g). The resulting SNR values are recorded in Table 3, which implies that the proposed algorithm is insensitive to $\rho_1, \rho_2$ and empirically $\rho_3 = 0.02$ gives better results.

**6. Conclusion.** In this paper, we proposed a total variation regularization model to recover an image from its partial and noisy magnitude information. We found that non-integer values when generating the structured illuminating data is key to

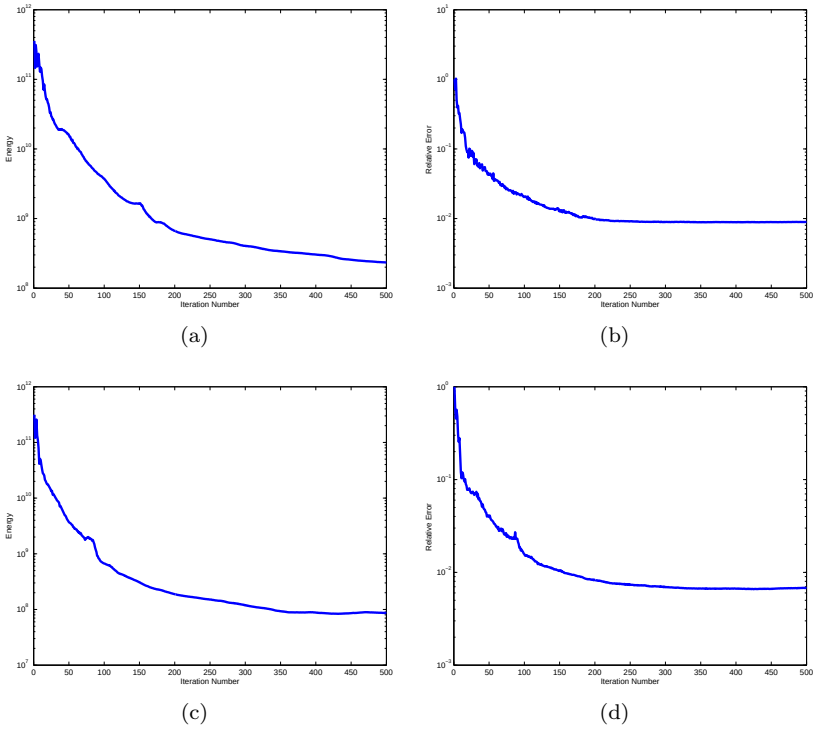


FIG. 10. *(a) and (c): Decreasing energies of* 10% *and* 30% *sampling for the example in Figure 8; (b) and (d): Corresponding relative errors.*

| | | | | | | |
|---|---|---|---|---|---|---|
| Different $\lambda$ | $\lambda$ | 10 | $10^2$ | $10^3$ | $10^4$ | $10^5$ |
| | SNR | 18.70 | 19.07 | **19.29** | 19.07 | 19.13 |
| Different $\rho_1$ | $\rho_1$ | $10^{-3}$ | $10^{-2}$ | 0.1 | 1 | 10 |
| | SNR | 13.52 | 16.97 | **19.29** | 16.53 | 15.75 |
| Different $\rho_2$ | $\rho_2$ | $10^{-3}$ | $10^{-2}$ | 0.1 | 1 | 10 |
| | SNR | 19.20 | 18.80 | **19.29** | 18.77 | 14.94 |
| Different $\rho_3$ | $\rho_3$ | $2\times10^{-4}$ | $2\times10^{-3}$ | $2\times10^{-2}$ | 0.2 | 2 |
| | SNR | 8.18 | 13.60 | **19.29** | * | 3.98 |

TABLE 3
*Parameters sensitivities (* means the algorithm blows up with the given parameters).*

stable phase recovery compared to the integers used conventionally [7]. The use of TV regularization helped to maintain image quality when only a small number of measurements are available. The ADMM is adopted to solve the proposed model efficiently, which is rather robust to initialization and model parameters. The recovered results are of better image quality, with at least 4dB increase in SNR values, compared to the classic least-square type of method. Moreover, the images reconstructed by our proposed method exhibit sharper edges and less artifacts.

Through experiments, we observe that both $s_1 = s_2 = 1/2$ and $[0, 1]$ box constraint are rather important to the exact/stable recovery. If $s_1, s_2$ are chosen to be other real numbers, the results are found to be much worse than that of $s_1 = s_2 = 1/2$. On the other hand, the box constraint is theoretically unnecessary to guarantee the so-

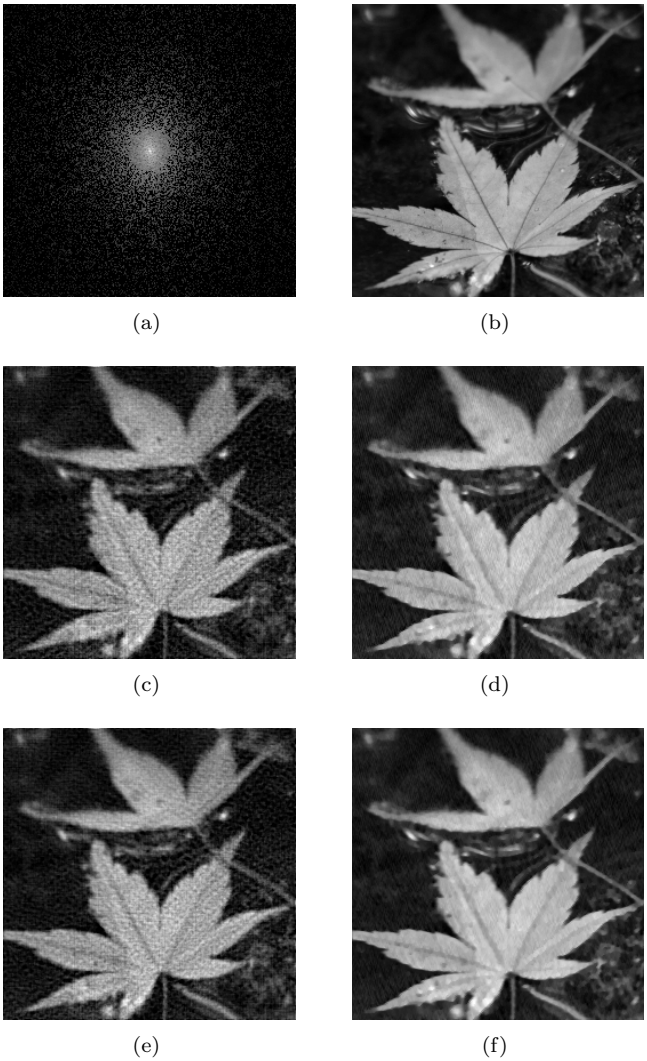

FIG. 11. *(a): 30% mask; (b): Original image (Resolution:* $256 \times 256$*); (c): phase retrieval by LSB with SNR=15.60 from noisy data (SNR=30 for noisy data); (d): phase retrieval by TVB with SNR=19.72; (e): phase retrieval by LSB with SNR=16.95 from noisy data (SNR=40 for noisy data); (f): phase retrieval by TVB with SNR=21.85*

lution's uniqueness, but computationally it enforces the boundedness of the solution, and hence the iterative algorithm is less prone to blow-up. It is worth of a careful investigation on these two conditions and how they interact with the TV regularization in the future.

**Acknowledgment.** The authors would like to thank Dr. Irène Waldspurger in the Computer Science Department of École Normale Supérieure to help us to do the comparison with PhaseCut algorithm, Dr. Xiaodong Li in the Statistics Department of UC Davis for helpful discussion. The insightful comments by the two referees are very appreciated, which help to improve the paper greatly. Dr. H. Chang is partially supported by National Natural Science Foundation of China (NSFC 11426165 and

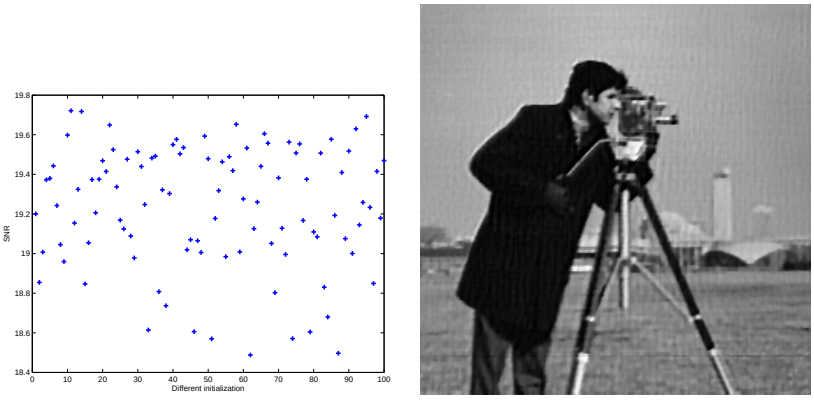


(a) (b)

FIG. 12. *(a): The SNR values of derived images by TVB with different initializations; (b): the average image derived by taking the average of all images with SNR=20.33.*

11501413) and Tianjin 131 Talent Project. Dr. Y. Lou is partially supported by NSF DMS-1522786.

**Appendix: Proof of Theorem 2.2.** *Proof.* First we consider it in 1-D cases, i.e. $u = (u_0, u_1, \ldots, u_{n-1})^T \in \mathbb{R}^n$, and $u_k \geq 0, \forall 0 \leq k \leq n-1$. $3n$ measurements $M(u) = \{|\mathscr{F}u|, |\mathscr{F}(u + D^s u)|, |\mathscr{F}(u - \mathbf{i}D^s u)|\}$ are known, where $\mathscr{F}$ denotes the 1-D discrete Fourier transformation, and $(D^s u)_k = \exp(\mathbf{i}\pi k/n)u_k$.

Since $u$ is real-valued, and define $U = (U_0, U_1, \ldots, U_{n-1})^T := \mathscr{F}u$, one has

$$U = (U_0, U_1, U_2, U_3, \ldots, \bar{U}_3, \bar{U}_2, \bar{U}_1)^T, \tag{6.1}$$

where $\bar{z}$ denotes the complex conjugate of $z$. Define

$$v = (v_0, v_1, \ldots, v_{n-1})^T := D^s u, V = (V_0, V_1, \ldots, V_{n-1})^T := \mathscr{F}v.$$

One readily has

$$V = (V_0, \bar{V}_0, V_2, V_3, \ldots, \bar{V}_4, \bar{V}_3, \bar{V}_2)^T, \tag{6.2}$$

since $V_1 = \bar{V}_0$, and $V_{n+1-k} = \bar{V}_k, \forall 2 \leq k \leq n-1$ (it could be readily verified only from the definitions).

Next we will study how to solve $U$ and $V$ from the measurements based on the the representations of $U, V$ in (6.1) and (6.2). As the triple $(|U_0|, |U_0 + V_0|, |U_0 - \mathbf{i}V_0|)$ is known, and $U_0$ is non-negative real-valued, we can solve $U_0, V_0$ if $U_0 \neq 0, V_0 \neq 0$. Similarly, by another triple $(|\bar{U}_1|, |\bar{U}_1 + \bar{V}_0|, |\bar{U}_1 - \mathbf{i}\bar{V}_0|)$, we can also obtain $U_1$ if $U_1 \neq 0$. Repeatedly, we can obtain $\bar{V}_2$ by the triple $(|\bar{U}_1|, |\bar{U}_1 + \bar{V}_2|, |\bar{U}_1 - \mathbf{i}\bar{V}_2|)$ if $V_2 \neq 0$. In a similar manner, one can sequentially obtain

$$U_0 \to V_0(= \bar{V}_1) \to U_1 \to V_2 \to U_2 \to \ldots \to U_{(n-1)/2} \to V_{(n+1)/2}, \text{if } n \text{ is odd};$$
$$U_0 \to V_0(= \bar{V}_1) \to U_1 \to V_2 \to U_2 \to \ldots \to V_{n/2} \to U_{n/2}, \text{if } n \text{ is even}.$$

By inverse Fourier transformation of $U$, one finally recovers the exact solution $u = \mathscr{F}^* U$.

For the 2-D cases, same notations $u, v \in \mathbb{R}^{n_1 \times n_2}$ are used, and associated DFTs are $U$ and $V$ respectively (Here we use the matrix form to represent their DFTs). Similarly to the 1-D cases, we have

$$\begin{aligned} &U_{k_1,k_2} = \bar{U}_{\mod(n_1-k_1,n_1),\ \mod(n_2-k_2,n_2)}, \\ &V_{k_1,k_2} = \bar{V}_{\mod(n_1+1-k_1,n_1),\ \mod(n_2+1-k_2,n_2)}, \forall 0 \le k_i \le n_i - 1. \end{aligned} \tag{6.3}$$

Similarly to the proof for the 1-D case, we start to compute the element from the index $(0,0)$, i.e. $U_{0,0} > 0$. First we get $V_{0,0}$ if $V_{0,0} \neq 0$. Repeatedly we find elements from $U$ and $V$ in turn. The indexes for the elements are determined by (6.3) so that the following sequences are generated as

$$\begin{array}{lccccccc} U: & U_{i_0,j_0} & & U_{i_1,j_1} & \longrightarrow & U_{i_2,j_2} & & U_{i_3,j_3} \longrightarrow \ \ldots \\ & \downarrow & & \uparrow & & \downarrow & & \uparrow \qquad\quad \ldots \\ V: & V_{i_0,j_0} & \longrightarrow & V_{i_1,j_1} & & V_{i_2,j_2} & \longrightarrow & V_{i_3,j_3} \qquad \ldots \end{array} \tag{6.4}$$

where

$$\begin{aligned} i_{2k+2} &= \mod(n_1 - i_{2k+1}, n_1), \qquad j_{2k+2} = \mod(n_2 - j_{2k+1}, n_2), \\ i_{2k+1} &= \mod(n_1 + 1 - i_{2k}, n_1), \qquad j_{2k+1} = \mod(n_2 + 1 - j_{2k}, n_2),\ \forall k = 0, 1, 2, \ldots. \end{aligned} \tag{6.5}$$

By (6.5), one can derive

$$i_{2k+2} = \mod(i_{2k} - 1, n_1), \qquad j_{2k+2} = \mod(j_{2k} - 1, n_2), \tag{6.6}$$

for arbitrary non-negative integers $k$.

We construct a set

$$\mathcal{S} := \{(i_{2k}, j_{2k}) |\ k = 0, 1, 2, \ldots, n_1 \times n_2 - 1\},$$

which is actually the index set by selecting some components of $U$ by (6.4). If one can prove that the cardinality of $\mathcal{S}$ is equal to be $n_1 \times n_2$, the proof will be completed starting from $U_{0,0}$. Let us first prove the cardinality of $\mathcal{S}$ is equal to be $n_1 \times n_2$ by contradiction. Assume there exist two identical elements $(i_{2k_0}, j_{2k_0}) \in \mathcal{S}$ and $(i_{2k_1}, j_{2k_1}) \in \mathcal{S}$, with $0 \le k_0 < k_1 \le n_1 \times n_2 - 1$. Noting that the elements of $\mathcal{S}$ satisfy (6.6), one has

$$i_{2k_0} = i_{2k_1} = \mod(i_{2k_0} - (k_1 - k_0), n_1), \qquad j_{2k_0} = j_{2k_1} = \mod(j_{2k_0} - (k_1 - k_0), n_2).$$

There exist two integers $a, b$, such that

$$i_{2k_0} - (k_1 - k_0) = a \times n_1 + i_{2k_0}, \qquad j_{2k_0} - (k_1 - k_0) = b \times n_2 + i_{2k_0}.$$

One readily deduces $k_1 - k_0 = -a \times n_1 = -b \times n_2$, i.e.

$$\mod(k_1 - k_0, n_1 \times n_2) = 0,$$

as $n_1$ is prime with $n_2$. Therefore $k_0 = k_1$, that leads to the contradiction with $k_0 < k_1$. Then one can claim that $\mathcal{S}$ consists of all the indexes of $U$. That concludes to this theorem. □

REFERENCES


[1] R. Balan, P. Casazza, and D. Edidin, *On signal reconstruction without phase*, Applied and Computational Harmonic Analysis, 20 (2006), pp. 345–356.

[2] H. H. Bauschke, P. L. Combettes, and D. R. Luke, *Phase retrieval, error reduction algorithm, and fienup variants: a view from convex optimization*, J. Opt. Soc. Amer. A, 19 (2002), pp. 1334–1345.

[3] ———, *Hybrid projectioncreflection method for phase retrieval*, J. Opt. Soc. Amer. A, 20 (2003), pp. 1025–1034.

[4] A. Beck and M. Teboulle, *A fast iterative shrinkage-thresholding algorithm for linear inverse problems*, SIAM journal on imaging sciences, 2 (2009), pp. 183–202.

[5] S. Boyd, N. Parikh, E. Chu, B. Peleato, and J. Eckstein, *Distributed optimization and statistical learning via the alternating direction method of multipliers*, Foundations and Trends® in Machine Learning, 3 (2011), pp. 1–122.

[6] E. Candés and T. Tao, *Near-optimal signal recovery from random projections: Universal encoding strategies?*, IEEE Trans. Inform Theory, 52 (2006), pp. 5406–5425.

[7] E. J. Candés, Y. C. Eldar, T. Strohmer, and V. Voroninski, *Phase retrieval via matrix completion*, SIAM J. Imaging Sci., 6 (2013), pp. 199–225.

[8] E. J. Candes, X. Li, and M. Soltanolkotabi, *Phase retrieval via wirtinger flow: Theory and algorithms*, IEEE Trans. Inf. Theory, 61 (2015), pp. 1985–2007.

[9] E. J. Candes, T. Strohmer, and V. Voroninski, *Phaselift: Exact and stable signal recovery from magnitude measurements via convex programming*, Commu. Pure Applied Math., 66 (2013), pp. 1241–1274.

[10] R. H. Chan, M. Tao, and X.M. Yuan, *Constrained total variational deblurring models and fast algorithms based on alternating direction method of multipliers*, SIAM J. Imaging Sci., 6 (2013), pp. 680–697.

[11] H. Chang, X.-C. Tai, L.-L. Wang, and D. Yang, *Convergence rate of overlapping domain decomposition methods for the rudin-osher-fatami model based on a dual formulation*, SIAM J. Image Sci., 8 (2015), pp. 564–591.

[12] Y. Chen and E. J. Candes, *Solving random quadratic systems of equations is nearly as easy as solving linear systems*, arXiv preprint arXiv:1505.05114, (2015).

[13] A. Conca, D. Edidin, M. Hering, and C. Vinzant, *An algebraic characterization of injectivity in phase retrieval*, Applied and Computational Harmonic Analysis, 38 (2015), pp. 346–356.

[14] J.C. Dainty and J.R. Fienup, *Phase retrieval and image reconstruction for astronomy*, Image Recovery: Theory and Application, ed. by H. Stark, Academic Press, (1987), pp. 231–275.

[15] V. Elser, *Phase retrieval by iterated projections*, J. Opt. Soc. Am. A, 20 (2003), pp. 40–55.

[16] A. Fannjiang, *Absolute uniqueness in phase retrieval with random illumination*, Inverse Probl., 28 (2012), p. 075008.

[17] A. Fannjiang and W. Liao, *Phase retrieval with random phase illumination*, J. Opt. Soc. Am. A, 29 (2012), pp. 1847–1859.

[18] ———, *Fourier phasing with phase-uncertain mask*, Inverse Probl., 29 (2013), p. 125001.

[19] J. R. Fienup, *Phase retrieval algorithms: a comparison*, Appl. Opt., 21 (1982), pp. 2758–2769.

[20] J. R. Fienup and C. C. Wackerman, *Phase-retrieval stagnation problems and solutions*, J. Opt. Soc. Am. A, 3 (1986), pp. 1897–1907.

[21] F. Fogel, I. Waldspurger, and A. d'Aspremont, *Phase retrieval for imaging problems*, arXiv preprint arXiv:1304.7735, (2013).

[22] R. W. Gerchberg and W. O. Saxton, *A practical algorithm for the determination of the phase from image and diffraction plane pictures*, Optik, 35 (1972), pp. 237–246.

[23] R. Glowinski and P. L. Tallec, *Augmented Lagrangian and operator-splitting methods in nonlinear mechanics*, SIAM Studies in Applied Mathematics, Society for Industrial and Applied Mathematics (SIAM), Philadelphia, PA, 1989.

[24] T. Goldstein and S. Osher, *The split Bregman method for L1-regularized problems*, SIAM J. Imaging Sci., 2 (2009), pp. 323–343.

[25] J.W. Goodman, *Introduction to Fourier Optics, Third Version*, Robert and Company Publishers, Englewood, 2005.

[26] M. Hayes, *The reconstruction of a multidimensional sequence from the phase or magnitude of its fourier transform*, IEEE Trans. Acoust. Speech Signal Process., 30 (1982), pp. 140–154.

[27] B. He and X. Yuan, *On the o(1/n) convergence rate of the douglas-rachford alternating direction method*, SIAM Journal on Numerical Analysis, 50 (2012), pp. 700–709.

[28] K. Kreutz-Delgado, *The complex gradient operator and the CR-calculus*, arXiv preprint, (2009).

[29] F. Li, S. Osher, J. Qin, and M. Yan, *A multiphase image segmentation based on fuzzy membership functions and l1-norm fidelity*, CAM report No. 15-21, (2015).
[30] D. R. Luke, *Relaxed averaged alternating reflections for diffraction imaging*, Inverse Probl., 21 (2005), pp. 37–50.
[31] D. R. Luke, J. V. Burke, and R. G. Lyon, *Optical wavefront reconstruction: Theory and numerical methods*, SIAM review, 44 (2002), pp. 169–224.
[32] M. Lustig, *SparseMRI v0.2*. `http://www.eecs.berkeley.edu/~mlustig/Software.html`.
[33] M. Lustig, D.L. Donoho, J. M. Santos, and J. M. Pauly, *Compressed sensing mri*, IEEE Signal Processing Magazine, 25 (2008), pp. 72–82.
[34] S. Marchesini, *Phase retrieval and saddle-point optimization*, J. Opt. Soc. Am. A, 24 (2007), pp. 3289–3296.
[35] J. Miao, H. N. Chapman, and D. Sayre, *Image reconstruction from the oversampled diffraction pattern*, Microscopy Microanalysis, 3 (1997), pp. 1155–1156.
[36] J. Miao, T. Ishikawa, Q. Shen, and T. Earnest, *Extending x-ray crystallography to allow the imaging of noncrystalline materials, cells, and single protein complexes*, Annu Rev Phys Chem., 59 (2008), pp. 387–410.
[37] J. Miao, J. Kirz, and D. Sayre, *The oversampling phasing method*, Acta Cryst., D56 (2000), pp. 1312–1315.
[38] R. Remmert, *Theory of complex functions*, Springer-Verlag, 28 (1991).
[39] L. Rudin, S. Osher, and E. Fatemi, *Nonlinear total variation noise removal algorithm*, Phys. D, 60 (1992), pp. 259–268.
[40] J. L. C. Sanz, *Mathematical considerations for the problem of fourier transform phase retrieval from magnitude*, SIAM J. Appl. Math., 45 (1985), pp. 651–664.
[41] Y. Shechtman, Y. C. Eldar, O. Cohen, H. N. Chapman, J. Miao, and M. Segev, *Phase retrieval with application to optical imaging: a contemporary overview*, Signal Processing Magazine, IEEE, 32 (2015), pp. 87–109.
[42] I. Waldspurger, A. Aspremont, and S. Mallat, *Phase recovery, maxcut and complex semidefinite programming*, Math. Program., Ser. A, (DOI 10.1007/s10107-013-0738-9, 2012), pp. 1–35.
[43] A. Walther, *The question of phase retrieval in optics*, Journal of Modern Optics, 10 (1963), pp. 41–49.
[44] Z. Wen, C. Yang, X. Liu, and S. Marchesini, *Alternating direction methods for classical and ptychographic phase retrieval*, Inverse Probl., 28 (2012), p. 115010.
[45] C. Wu and X.-C. Tai, *Augmented Lagrangian method, dual methods and split-Bregman iterations for ROF, vectorial TV and higher order models*, SIAM J. Imaging Sci., 3 (2010), pp. 300–339.
[46] Y. Xu, W. Yin, Z. Wen, and Y. Zhang, *An alternating direction algorithm for matrix completion with nonnegative factors*, Frontiers of Mathematics in China, 7 (2012), pp. 365–384.
[47] P. Yin and J. Xin, *Phaseliftoff: an accurate and stable phase retrieval method based on difference of trace and frobenius norms*, Comm. Math. Sci., 13 (2015), pp. 1033–1049.